# INVESTIGATION OF SINGLE-SIDED TIG WELDING IN DISSIMILAR AISI 316L AND 304L STAINLESS STEEL JOINTS

S. Senthil Murugan[1,*], S. Kattimani[2],
R. Saminathan[3], M. J. I. Raj[4]

[1]Department of Mechanical Engineering, Sri Venkateswara College of Engineering (Autonomous), Tamil Nadu, India
[2]Department of Mechanical Engineering, National Institute of Technology, Karnataka, India
[3]Department of Mechanical Engineering, College of Engineering and Computer Science, Jazan University, Jazan, Saudi Arabia
[4]Department of Mechanical Engineering, Mar Ephraem College of Engineering and Technology, Tamil Nadu, India
[*]Corresponding author's e-mail address: gctsegan@gmail.com

## ABSTRACT

*This study investigates the Tungsten Inert Gas (TIG) welding of dissimilar austenitic stainless steels, AISI 304L and AISI 316L, each with a thickness of 3.2 mm. A single-pass butt joint was welded using a 100 A current with argon shielding gas. The joints underwent mechanical testing, including tensile, bend, impact, and hardness tests. The tensile test revealed a 25% reduction in the weld joint strength compared to the base metal, primarily due to differences in thermal expansion and mechanical properties, resulting in an overall joint efficiency of 75%. Macro and microstructural analyses indicated good fusion without defects, and typical weld metal microstructures were observed. The heat-affected zone (HAZ) of AISI 304L showed larger grains, while AISI 316L exhibited a flaky structure. The hardness test indicated the highest value in the weld zone (191 HV), compared to the HAZ (177 HV) and the parent metal (170 HV), which can be attributed to grain refinement and the use of the SS304 filler rod. Impact tests demonstrated good impact resistance (45 J), with the HAZ exhibiting higher toughness compared to the parent metal. Bend tests revealed no cracks on the weld face, whereas cracks were observed in the root bend tests. The study demonstrated sufficient strength, toughness, and hardness in the dissimilar TIG joint for engineering applications, despite the reduced tensile strength compared to the base metals.*

**KEYWORDS:** dissimilar welding, TIG, AISI 316, AISI 304, mechanical property, microstructure

## 1. INTRODUCTION

The growing demand for durable and corrosion-resistant materials in the transportation industry, particularly for metro rail fabrication, has led to the increased use of austenitic stainless steels like AISI 316L and AISI 304L. These alloys are favoured for their excellent mechanical properties, oxidation resistance, and weldability. AISI 316L, enriched with molybdenum, offers superior corrosion resistance, particularly in chloride environments, and demonstrates enhanced protection against crevice and pitting corrosion, making it a preferred choice over AISI 301L in metro rail applications. It is highly durable in harsh conditions, while AISI 304L serves as a more cost-effective alternative, providing good mechanical performance and corrosion resistance [1]. These stainless-steel grades are commonly used in metro rail applications, including components such as car bodies, fasteners, seats, and doors, due to their excellent corrosion resistance, making them highly suitable for environments with exposure to moisture, humidity, and corrosive substances.

Austenitic stainless steels, known for their high austenite content, resist intergranular corrosion and are non-magnetic, making them ideal for industries such as pharmaceuticals, household goods, marine, aerospace, food processing, heat exchangers, boiler tubes, metro rail, and chemical applications [2-5]. The Delhi Metro Rail Corporation (DMRC) of India has developed commuter-friendly coaches using 300 series stainless steel [6]. In metro rail carriages exposed to rain, humidity, and cleaning agents, AISI 304L prevents corrosion and resists discolouration and staining [7].

© *Galati University Press, 2025*

Date of submission/acceptance: 26.05.2025/15.12.2025
https://doi.org/10.35219/awet.2025.03

Both AISI 304L and AISI 316L are easy to clean, durable, and can withstand heat from sunlight and exposure to salty or corrosive substances, making them ideal for interior and exterior components of metro rail carriages, outperforming AISI 301 steels.

Different applications often demand specific material properties, such as strength, corrosion resistance, and conductivity, which may not be achievable with a single material [8]. Combining dissimilar alloys in metro rail applications ensures optimal performance, durability, and safety in various environments. However, welding dissimilar joints between these stainless-steel grades presents challenges in maintaining mechanical properties and corrosion resistance in the weld zone. Metro rail carriages require high standards of durability, corrosion resistance, and structural strength, demanding the adaptation of welding techniques to meet these stringent requirements. TIG and MIG welding are widely used for joining similar and dissimilar ferrous alloys in industries such as aerospace, automotive, and nuclear, where weld integrity is critical [9-12].

TIG welding is commonly used for joining stainless steels due to its precision, ability to control heat input, and capacity to produce high-quality welds with minimal distortion [13]. Despite its advantages, TIG welding can influence the microstructure and mechanical properties of the welded joint, potentially leading to issues like intermetallic phases, carbide precipitation, and HAZ sensitization. TIG welding is particularly suited for producing high-quality welds on materials with thicknesses up to 8 mm, making it ideal for sheet material, despite being relatively slower than other welding methods [10, 11].

Recent studies indicate that GTAW is highly effective for fabricating double-butt joints in SS304, particularly at a current of 97 A. The various numerical analysis techniques can enable the evaluation of residual stresses, strength, and thermal effects during the GTAW welding of AISI 316L alloy [14-17]. Similarly, AI algorithms now predict optimal welding parameters and weldment microstructures, with AI-GTAW methods aiding in material joining [18]. The activated tungsten inert gas welding process (ATIG) showed superior performance in joining dissimilar austenitic stainless steels [11], [19]. Kumar A.S et al. [20] highlighted the critical role of welding current in penetration depth and weld zone characteristics, noting that increased current reduced tensile strength while welding SS316L using submerged arc welding process.

Feng Yueqiao et al. [12] studied the welding of 10 mm thick AISI 316L alloy using the keyhole gas tungsten arc welding (KGTAW) process, demonstrating that single-pass welding of 10 mm thickness is achievable with GTAW. The weld exhibited mechanical properties comparable to the base metal, with improved corrosion resistance. Fei Z. et al. [21] investigated the effect of post-weld heat treatment on butt joints of P91 and AISI 316L alloys welded using the GTAW process. Their findings revealed superior tensile strength compared to electron beam welding (EBW). Additionally, ultrasonic water jet technology has demonstrated the potential to improve the mechanical properties of GTAW joints, with reported enhancements of 30–40% [22]. Shao Ling et al. [23] used ultra-pulse frequency GTAW to join titanium alloys, achieving 72% joint efficiency. Muzamil M. et al. [24] enhanced the mechanical properties of aluminium butt joints using carbon nanotube-assisted GTAW, while a hybrid GTAW-WAAM process was applied to Mg-Li alloys, showing the WAAM current's role in grain refinement [25, 26].

This study investigates the impact of single-pass TIG welding on the microstructure and mechanical properties of dissimilar AISI 316L/304L joints, focusing on metro rail applications. Emphasizing efficiency and cost-effectiveness, the research evaluates welds for minimal distortion and defects, providing insights for reliable, high-performance dissimilar butt joints tailored to metro rail needs.

## 2. MATERIALS AND METHODS

In this study, TIG welding was employed to join two dissimilar plates, austenitic stainless steels AISI 304L and AISI 316L (L means Low carbon content, less than or equal to 0.03 %). AISI 304L is suited for general-purpose corrosion resistance, while AISI 316L is preferred for harsher chemical or chloride-rich environments. The chemical composition of both base metals (BM) is presented in table 1. The presence of the Mo element is noted in AISI316L alloy. Two plates of size 150 mm x 230 mm x 3.2 mm were used as BM. Before welding, it is essential to thoroughly clean the surfaces of the materials to remove contaminants, oils, or oxides to ensure a strong, clean weld [27]. The experiment involved single-pass butt welding along one side of the workpiece. The two plates were positioned closely without any gap. During the welding process, current of 100 A, voltage of 12 V, welding speed of 1.0 mm/s, and argon gas flow rate of 18 l/min were set and applied. Argon served as the shielding gas to prevent oxidation and undesirable reactions that could compromise the weld quality.

The tungsten electrode, with a diameter of 3.0 mm, created an electric arc when brought near the workpieces, generating the heat required to melt both the base metals and the filler rod (SS304). The molten metal formed a weld pool in the joint area, and a filler rod was manually added to strengthen the joint and fill any gaps to form a strong joint. The welded joint and its front view with the weld bead mounted on a mould are depicted in figures 1a and 1b. Specimens were cut, as per the standard, from the welded plates using a wire EDM machine for sample preparation for further testing and microstructural characterisation. The precise control provided by the TIG welding process enabled fine-tuning of parameters such as arc current, voltage, and travel speed to optimize weld bead shape,

penetration depth, and overall quality. Electro-etching was performed using a 10 % oxalic acid solution, which helped to reveal the weld structure by converting insoluble iron into soluble iron. ASTM E8 standard was followed for taking tensile test trials of weld joints. Optical microscopy was used for the macro and microstructure analysis. Vickers microhardness tests were performed in accordance with the ASTM E384 standard, using a 0.3 kg applied load with 10 seconds dwell time. Charpy impact tests were conducted on the welded specimen following ASTM E23 standard.

**Table 1.** Chemical composition of AISI 304L and 316L Stainless steel

| Element | C | Mn | P | S | Si | Cr | Ni | N | Fe | Mo |
|---|---|---|---|---|---|---|---|---|---|---|
| AISI 304L (wt%) | 0.03 | 2 | 0.045 | 0.015 | 1.0 | 18 | 9.5 | 0.10 | 69.31 | -- |
| AISI 316 L (wt%) | 0.03 | 2 | 0.045 | 0.030 | 1.0 | 17 | 14 | 0.10 | 62.79 | 3 |

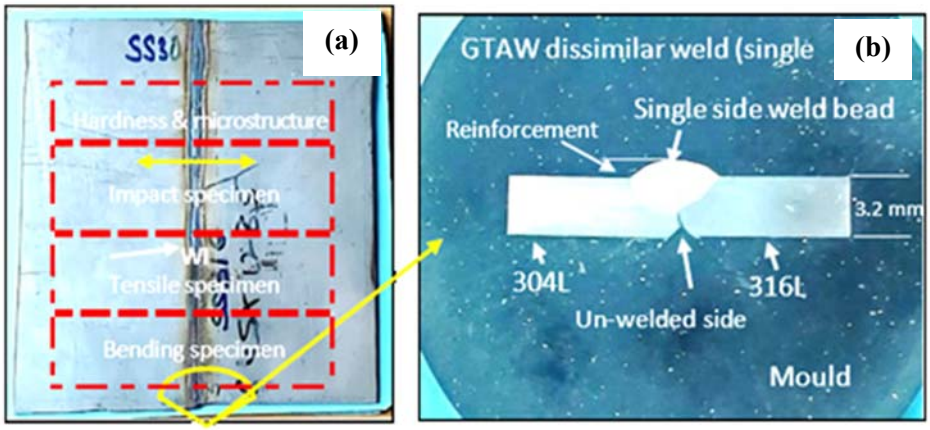


**Fig. 1.** The welded joint: a) prepared dissimilar weld joint; b) prepared specimen on a mould for macrograph and showing weld bead

## 3. RESULTS AND DISCUSSION

### 3.1. Macro and Microstructure

A macro-examination of the dissimilar AISI 304L/AISI 316L single-side TIG-welded joint revealed sound fusion characteristics without any observable weld defects such as porosity or solidification cracks (Fig. 2a). The weld face exhibited a slight reinforcement of approximately 1 mm, with a maximum penetration depth of 1.5 mm and an overall bead width of approximately 4 mm. Although complete root fusion was not achieved due to the single-sided welding configuration, the weld cross-section confirmed uniform bead geometry with no major discontinuities.

The microstructural features of the joint are presented in figures 2b-d. The base metals (AISI 304L and AISI 316L) displayed typical austenitic stainless-steel microstructures characterised by annealed twin boundaries within the austenitic matrix.

In the fusion zone, an interdendritic austenitic structure was observed, which is commonly associated with rapid solidification in stainless-steel welds [6, 9-11, 28]. Closer examination of the weld interface (WI) in figure 2b) highlighted the distinct heat-affected zones (HAZ) on both sides of the joint.

On the AISI 304L side, the HAZ exhibited coarser grains with an average grain size of ~45–50 µm, while the AISI 316L side showed partially recrystallised grains averaging ~18–20 µm, reflecting different thermal responses due to variations in alloy composition and thermal conductivity. The observed microstructural differences between the two alloys can be attributed to their distinct metallurgical characteristics under the same heat input. The refinement of grains adjacent to the weld interface indicates localised rapid solidification, whereas the coarsening in the 304L HAZ suggests prolonged thermal exposure.

No evidence of carbide precipitation or secondary phases was detected under optical microscopy, indicating limited sensitization under the applied welding conditions. These microstructural features confirm that TIG welding produced a defect-free fusion zone with refined grains near the weld interface, though incomplete penetration at the root remains a process-related limitation of single-side welding.

Overall, the microstructural analysis demonstrates that dissimilar joining of AISI 304L and AISI 316L facilitates the formation of hybrid regions with tailored properties, which can be further optimised through post-weld heat treatment to refine grains and stabilised phases [29]. With controlled TIG parameters, the welded joints are expected to achieve adequate

mechanical performance and reliability, making them suitable for critical applications such as metro rail fabrication, where precise control of material integrity is essential.

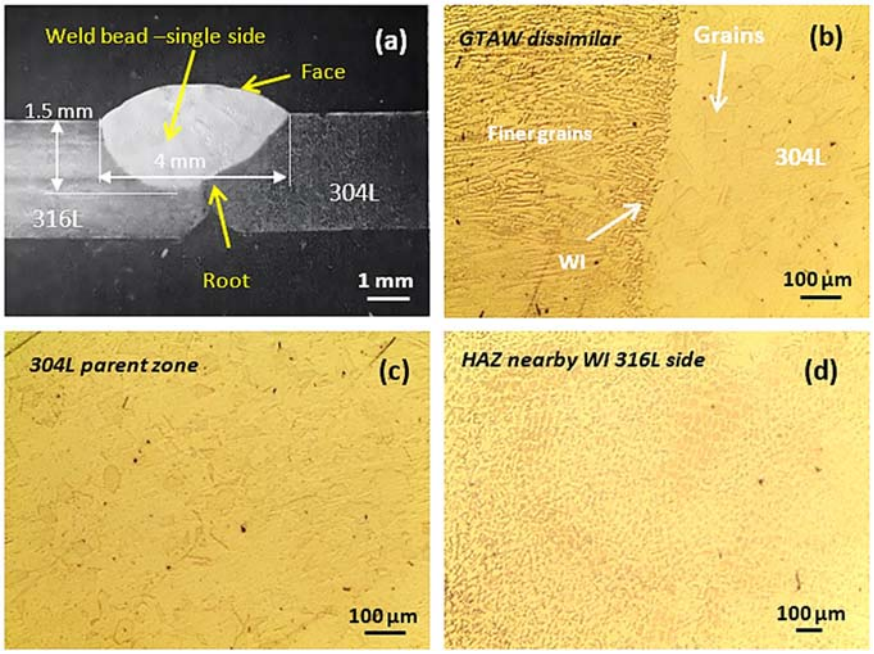


**Fig. 2.** Macro and microstructure: a) macrograph of dissimilar weld with weld bead; b) microstructure of WI of dissimilar joint; c) microstructure of BM; d) HAZ nearby WI and grains

## 4. MECHANICAL PROPERTIES

### 4.1. Tensile Strength and Joint Performance

Tensile tests were conducted on all joints to determine their tensile strength (TS) using a Universal Testing Machine (UTM). The results from these tests are presented in figure 3 and table 2. The breakage occurred in the weld zone, although the ductile behaviour of the weld zone was still evident. Figure 3 shows the load-displacement curve, indicating that the dissimilar joint sustained a maximum load of 14.9 kN until a displacement of 1.2 mm. Beyond this point, the load gradually decreased. The ultimate load was reached at a displacement of 1.2 mm, with the maximum displacement recorded at 1.5 mm. Table 2 shows the peak load response of the joint and the tensile strength of the dissimilar 316L/304L. The TIG-welded joint was measured to be approximately 360 MPa. This is lower than the strength of the base metals (AISI 304L: ~580 MPa, AISI 316L: ~610 MPa), indicating that the weld zone is mechanically weaker due to incomplete root fusion and microstructural discontinuities. Upon comparing the tensile values between the base metals (AISI 316L and AISI 304L) and the dissimilar joint, it was found that the tensile strength of the joint, with a single-side weld pass, was approximately 25 % lower than the base metals. This corresponded to a joint efficiency of 75 %, with the maximum tensile strength of the joint being 361 MPa. The joint efficiency was calculated by taking the ratio of the tensile strength of the weld joint to the tensile strength of the base metal with the lower strength (AISI 304L).

Several researchers have investigated TIG welding of AISI 316L and AISI 304L alloys, but limited studies exist on the dissimilar TIG joining of AISI 316L/304L. It is well-documented that TIG welding performance on microstructure and mechanical properties depends on plate thickness and welding parameters. Advanced techniques like Activated TIG (A-TIG) welding, using activated flux coatings, have been shown to enhance tensile strength, toughness, and bead geometry. Hedayat Mohammad Soltani and Morteza Tayebi [30] studied TIG welding of dissimilar AISI 304L to AISI 316L (1.0 mm thickness) and reported tensile strengths of 500–600 MPa. They observed that coarsening of solidification layers reduced strength and toughness, while finer microstructures from shielding gas improved strength. Conversely, high voltages during laser welding caused austenitic layer coarsening, leading to lower strength.

Rajaravi C et al. [31] achieved 600MPa tensile strength on 4 mm thick AISI 316L plates by optimizing TIG parameters, while Ghumman K.Z et al. [32] reported tensile strengths of 300-600 MPa for 3 mm thick AISI 316L plates under varying welding conditions. Ahmadi E and Ebrahimi A.R [33] found that A-TIG welding on 9 mm thick AISI 316L plates increased tensile strength to 600 MPa by enhancing delta-ferrite retention. These findings highlight the potential of A-TIG to improve weld strength in stainless steels.

The reduction in tensile strength was primarily attributed to differences in the thermal expansion coefficients between the two materials, which can cause residual stresses and distortions during welding. Furthermore, the TS of TIG joints is highly sensitive to several factors, including the material properties, welding parameters (e.g., current, voltage, and travel speed), filler material selection, and the skill of the welder. In this case, inconsistencies in travel speed, incorrect torch angles, and improper manipulation of the filler metal during the welding process likely contributed to the reduction in joint strength. Additionally, thermal stresses induced by the different expansion rates of AISI 304L and AISI 316L could lead to microstructural variations in the weld zone, further affecting mechanical properties. These factors highlight the complexity of achieving optimal tensile properties in dissimilar metal welds, particularly when joining materials with differing thermal and mechanical characteristics.

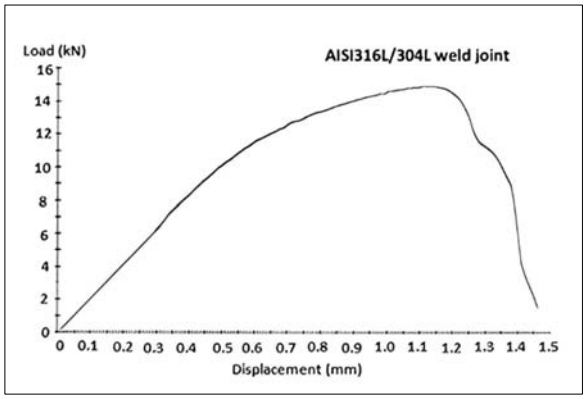


**Fig. 3.** Load-displacement graph of the tested weld specimen

**Table 2.** TIG welded AISI316L/304L joint

| Parameters | Values |
|---|---|
| Tensile strength (MPa) | 361 |
| Peak load (kN) | 14.9 |
| Joint efficiency (%) | 75 |

## 4.2. Bendability Test

This mechanical test is used to evaluate the ductility, structural integrity, flexibility, and deformation resistance of a welded joint without leading to fracture or failure. It plays a crucial role in assessing the quality of welds in manufacturing industries. In this study, the dissimilar weld samples underwent bend testing to evaluate their bending performance, and the results are given in table 3. Both the face and root bend tests were performed on the single-sided butt weld. The test involved bending the welded specimens to observe their behaviour under stress, including any signs of cracking, necking (localized narrowing), or other deformations. These observations help determine the material's ability to withstand stress before fracturing. The test continued until either the specimen fractured or reached the specified deformation limits as defined by testing standards.

During the bend test, a surface narrow-width crack was observed along the weld face (Fig. 4a, b), whereas a more pronounced crack, measuring about 2 mm in width, developed in the root region during the root bend test (Fig. 4c). Both cracks were oriented along the weld line**.** Such cracks represent critical discontinuities, as they can extend under cyclic or fluctuating loading and ultimately cause fracture. The bend angle achieved was approximately 160–165°**,** with an inner bend radius of about 5 mm, indicating that the welded joint retained a significant degree of plastic deformability before crack propagation. These results confirm that the weld exhibited adequate flexural strength and formability, though localised strain concentration at the weld/HAZ boundary reduced its bendability compared to the base material.

In the root bend test (Fig. 4c), a crack initiated from the weld root region, confirming that the root was not fully fused. Only localised bonding was evident at two points, while small cavities of ~0.2–0.4 mm were present near the weld root. These defects are characteristic of single-side TIG welding, where complete penetration is difficult to achieve because heat input is applied from only one side of the joint. The defects served as stress concentrators and led to a dominant. Although such imperfections reduced the bendability compared to the base metal, they reflect the realistic performance of single-side TIG-welded joints, which was the focus of this study.

## 4.3. Impact Energy

The Charpy test measures the energy absorbed in Joules (J) by the specimen of AISI316L/304L TIG dissimilar joint during fracture, providing insight into the joint's ability to resist impact forces. All Charpy specimens were prepared as sub-size V-notch specimens in accordance with ASTM E23.

Specimens measured 55 × 10 × 3.2 mm (L × W × t), with a 45° V-notch and 0.25 mm root radius. Notch depth was scaled proportionally from the standard 2.0 mm depth (i.e., 0.64 mm for 3.2 mm thickness) so that the notch geometry (angle and root radius) is maintained while the ligament varies as required for sub-size tests.

The notch position was selected to force crack propagation through the weld centreline. Testing was conducted at room temperature, and three trials were performed on different sections of the joint: the weld zone, HAZ, and BM.

During the test, the pendulum struck the notched specimen, causing a fracture. The energy absorbed by the specimen during the fracture event was recorded by the machine.

**Table 3.** Bendability test observations

| Bending test | Specimen | Observation |
|---|---|---|
| Face bend test (4t/180°) | AISI 316L/304L dissimilar single-sided TIG joint | Initiation of crack propagation |
| Root bend test (4t/180°) | | Major crack |

The results, illustrated in figure 5, reveal significant differences in impact energy absorption between the weld, HAZ, and BM. The weld zone demonstrated the highest impact resistance, absorbing a maximum of 45 J, indicating good toughness.

The HAZ exhibited higher energy absorption compared to the BM, with values of 39 J and 24 J, respectively. This suggests that the HAZ is tougher than the BM, likely due to microstructural changes induced by the welding process. The fracture occurred within the notched region, and plastic deformation was visible on the tested specimens, confirming that the dissimilar weld joint exhibited a reasonable degree of ductility in the BM and HAZ regions, unlike in the weld zone. Materials with higher Charpy impact values, as observed in the weld and HAZ, are generally considered more resistant to sudden loading or impact, reducing the likelihood of catastrophic failure under dynamic conditions. Pratishtha Sharma and Dheerendra Kumar Dwivedi [34] joined 8 mm thick dissimilar plates of AISI 304H and P92 steel using a single-pass A-TIG process. The weld zone of AISI 304H exhibited an average impact toughness of 30 J at a welding current of 220 A and a speed of 80 mm/min.

The results of this study highlight that the AISI 316L/304L dissimilar weld joint retains sufficient toughness, making it suitable for applications where impact resistance is critical, such as in metro rail fabrication, where the structure is subjected to varying dynamic stresses. This test also demonstrates that the proper control of welding parameters in the TIG process can optimize the toughness of the weld and HAZ, despite the challenges posed by the different thermal expansion properties of AISI 316L and AISI 304L.

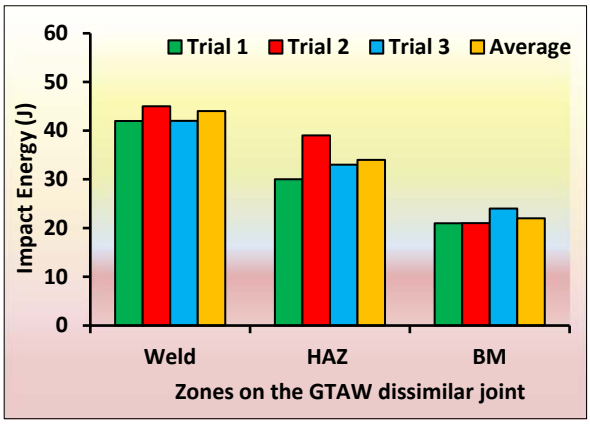


**Fig. 5.** Graphical representation of impact energy results

## 4.4. Vickers Microhardness

The microhardness profile of the TIG-welded AISI 316L/AISI 304L dissimilar joint was evaluated, and the results are presented in figure 6. The microhardness test was also performed on three distinct regions, like the weld zone, HAZ, and the BM on both sides. In this study, the maximum microhardness recorded was 191 HV in the weld zone, indicating the highest hardness of all tested areas. This elevated hardness in the weld zone is attributed to the finer grain structure formed as a result of rapid cooling following solidification during the welding process. The refined microstructure in the weld region enhances its hardness and mechanical strength. The HAZ exhibited a hardness value of 177 HV, which, although slightly lower than the weld zone, was still significantly higher than the parent metal or BM, which measured 170 HV. The increased hardness in the HAZ can be explained by the thermal cycles experienced during the welding process. The area adjacent to the weld pool in the HAZ is exposed to elevated temperatures, leading to microstructural changes. This thermal exposure can cause grain growth and transformation of phases in the stainless steel, contributing to an increase in hardness compared to the BM.

Baghel A. et al. [35] studied TIG welding of AISI 304L alloy (6 mm thick plate) and found that currents below 80 A did not achieve penetration, while currents above 120 A caused excessive melting. Current and welding speed were the most influential factors on Vickers hardness, with microhardness values ranging from 200–230 HV due to the formation of fine delta ferrite structures. Kuang-Hung Tseng and Chih-Yu Hsu [36] reported that A-TIG welding increased joint penetration and the weld depth-to-width ratio at a 200 A current. However, the addition of oxide flux had minimal impact on the hardness of AISI 316L (6 mm thick plate), which remained in the range of 185–190 HV. Hemant Kumar and N.K. Singh [37] observed similar hardness levels for conventional and A-TIG welded AISI 304L (8 mm thick plate), achieving 230 HV in the weld zone with a welding speed of 100 mm/min and a gas flow rate of 10 L/min. For AISI 316L (3 mm thick plate), Ghumman K.Z et al. [32] achieved optimum microhardness values of 250–300 HV using a parametric combination of 125 A current, 16 V voltage, and a 9 L/min gas flow rate. Rajaravi C et al. [31] reported hardness values of 175–190 HV, while Hedayat Mohammad Soltani et al. [30] recorded a maximum of 190 HV, highlighting the dependency on TIG welding parameters.

The solidification process in the weld zone involves rapid cooling, which limits grain growth and facilitates the formation of a finer, more uniform microstructure. This finer microstructure is directly responsible for the higher hardness in the weld zone compared to the HAZ and BM. Additionally, the presence of the SS304 filler rod used during the welding process played a significant role in the hardness profile of the weld zone. The filler material interacted with the BM, contributing to the formation of harder phases in the weld pool, thereby enhancing the hardness. In contrast, the BM exhibited the lowest hardness, as they were not subjected to the intense thermal gradients and metallurgical transformations seen in the weld zone and HAZ.

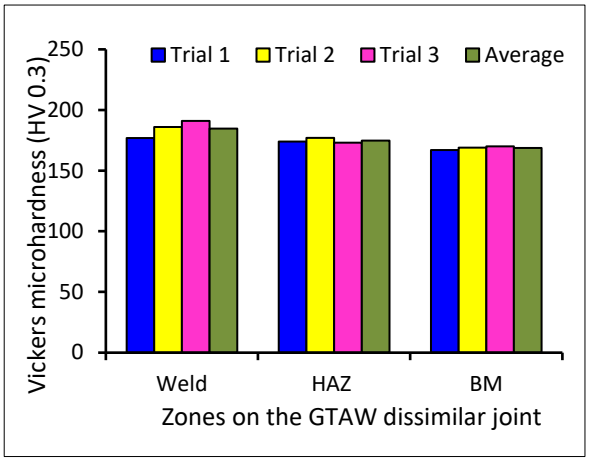


**Fig. 6.** Vickers microhardness results of weld, HAZ and parent metal zone

The gradual reduction in hardness from the weld zone to the BM is typical in dissimilar welding, where the mechanical properties of the welded joint are influenced by the microstructural evolution across these regions. Overall, the combination of thermal cycles, cooling rates, and the SS304 filler rod during the TIG process resulted in the observed hardness profile, with the weld zone displaying superior hardness due to its refined grain structure. This hardness distribution is essential for the mechanical performance of the welded joint in applications like metro rail fabrication, where the weld zone's mechanical integrity and durability are critical.

## 5. CONCLUSIONS

This study explored the mechanical and microstructural properties of a dissimilar TIG joint (single-sided butt joint) with AISI 304L and AISI 316L alloys. Weld bead with a maximum width of 4 mm and a depth of 1.5 mm ensured minimal material loss. The joint demonstrated reduced tensile strength (~25% lower than the AISI 316L BM), attributed to differences in thermal expansion and mechanical properties and withstood a maximum of 15 kN load. However, the weld exhibited good ductility and impact toughness, with a maximum recorded energy of 45 J in the weld zone. Microstructural analysis revealed a refined grain structure in the weld zone without cracks and defects, resulting in increased hardness (191 Hv) compared to the heat-affected zone (177 Hv) and parent metal (170 Hv). Annealed twin boundaries were found in the BM and interdendritic structures in the weld zone, which contributed to joint integrity. Bend tests confirmed sufficient flexibility and formability, although a crack appeared during the root bend test. Overall, the dissimilar TIG joint meets the mechanical performance requirements, making it suitable for applications in metro rail carriages and other engineering structures requiring corrosion resistance and mechanical durability.

## REFERENCES

[1] **Senthil Murugan S., Girisankar S., Devanathan C. et al.**, *Analysis of UNS S31603 ferrous joint made by rotary friction welding,* Sādhanā, vol. 49, 2024, p. 146.
[2] **Senthil Murugan S., Sathiya P.,** *Effect of innovative faying surfaces on dissimilar metal welds made with friction rotary joining,* Welding in the World, 2024, vol. 68, pp. 1769-1781.
[3] **Ghosh S., Kain V., Ray A. et al.,** *Deterioration in Fracture Toughness of 304L Austenitic Stainless Steel Due to Sensitization,* Metallurgical and Materials Transactions A, 2009, vol. 40, pp. 2938-2949.
[4] **Yan Zhang, Qizhe Ye, Yu Yan,** *Processing, microstructure, mechanical properties, and hydrogen embrittlement of medium-Mn steels: A review*, Journal of Materials Science & Technology, 2024, vol. 201, pp. 44-57.
[5] **Dongsheng Qian, Lingyan Wu, Feng Wang, Song Deng, Fei Yin, Shaofeng Jiang,** *Tailored carburization gradient microstructure and enhanced wear properties of M50NiL steel via introduced prior cold rolling,* Wear, 2024, pp. 540-541.
[6] ******* *A magazine on Stainless steel*, Indian Stainless Steel Development Association, ISSN: 0971-9482, vol. 12, iss. 3, 2007.
[7] **Selvakumar M., Ramulu D. S., Sankar K.,** *A Unique Metro Choice Behaviour of Suburban Rail Passengers in India*, Urban Rail Transit, vol. 9, 2023, pp. 31-41.
[8] **Senthil Murugan S., Sathiya P., Noorul Haq A.,** *Mechanical Properties Estimation from Tensile Testing of AA6063-AISI304L Bimetal Joints Friction Welded with Different Joining Methods*, Surface Review and Letters, 2021, vol. 28, iss. 4, 2150013.
[9] **Kumar R.,** *Study of GTAW welding on bi-metal weld AISI 304 and Monel 400*, Materials Today: Proceedings, 2021, vol. 37, iss. 2, pp. 3512-3515.
[10] **Tongov M., Dimitrova R., Konstantinov K.,** *Bead formation research in GTAW welding of AISI 304 steel*, IOP Conference Series: Materials Science and Engineering, 2020, vol. 878, 012054.
[11] **Kulkarni A., Dwivedi D. K., Vasudevan M.,** *Microstructure and mechanical properties of A-GTAW welded AISI 316L SS-Alloy 800 dissimilar metal joint*, Materials Science and Engineering: A, 2020, vol. 790, 139685.
[12] **Feng Y., Luo Z., Liu Z., Li Y., Luo Y., Huang Y.,** *Keyhole gas tungsten arc welding of AISI 316L stainless steel,* Materials & Design, 2015, vol. 85, pp. 24-31.
[13] **Kumar K., Kumar S. Ch., Masanta M., Pradhan S.,** *A review on GTAW welding technology variants and its effect on weld geometry*, Materials Today: Proceedings, 2022, vol. 50, iss. 5, pp. 999-1004.
[14] **Depradeux L., Jullien J. F.,** *2D and 3D Numerical Simulations of TIG Welding of a 316L Steel Sheet,* Revue Européenne Des Éléments Finis, 2004, vol. 13, iss. 3-4, pp. 269–288.
[15] **Arora H., Singh R., Brar G. S.,** *Numerical simulation on residual stresses of stainless-steel SS-304 thin welded pipe*, Measurement and Control, 2020, vol. 53, iss. 7-8, pp. 1183-1193.
[16] **Balram Y., Rajyalakshmi G.,** *Thermal fields and residual stresses analysis in GTAW weldments of SS 316 and Monel 400 by*

*numerical simulation and experimentation,* Materials Research Express, 2019, vol. 6, 0865e2.
[17] **Zhu Q. M., Chen J., Gou G., Chen H., Li P.,** *Ameliorated longitudinal critically refracted—Attenuation velocity method for welding residual stress measurement*, Journal of Materials Processing Technology, 2017, vol. 246, pp. 267-275.
[18] **Kesse M. A., Buah E., Handroos H., Ayetor G. K.,** *Development of an Artificial Intelligence Powered GTAW Welding Algorithm for the Prediction of Bead Geometry for GTAW Welding Processes using Hybrid Deep Learning*, Metals, 2020, vol. 10, iss. 4, 451.
[19] **Touileb K., Hedhibi A. C., Djoudjou R., Ouis A., Bensalama A., Ibrahim A. et al.,** *Mechanical, Microstructure, and Corrosion Characterization of Dissimilar Austenitic 316L and Duplex 2205 Stainless-Steel AGTAW Welded Joints*, Materials, 2020, vol. 5, 2470.
[20] **Kumar A. S., Sharma S. K. Shukla A. K,** *Microstructural, Mechanical, and Thermal Analysis of SS316L Weldment for Marine Engineering Application*, Journal of Materials Engineering and Performance, 2024, vol. 33, pp. 13502-13515.
[21] **Fei Z., Pan Z., Cuiuri D. et al.,** *Effect of post-weld heat treatment on microstructure and mechanical properties of deep penetration autogenous GTAW welded dissimilar joint between creep strength enhanced ferritic steel and austenitic stainless steel*, International Journal of Advanced Manufacturing Technology, 2020, vol. 108, pp. 3207–3229.
[22] **Srivastava M., Hloch S., Krejci L. et al.,** *Utilizing the water hammer effect to enhance the mechanical properties of AISI 304 welded joints*, International Journal of Advanced Manufacturing Technology, 2022, vol. 119, pp. 2317–2328.
[23] **Shao L., Zhang X., Chen Y., Zhu L., Wu S., Liu Q., Li W., Xue N., Tu Z., Wang T., Zhang J., Dai S., Shi X., Chen M.,** *Why do cracks occur in the weld joint of Ti-22Al-25Nb alloy during post-weld heat treatment?* Frontiers in Materials, 2023, vol. 10, 1135407.
[24] **Muzamil M., Wu J., Akhtar M., Zhang Z., Majeed A,. Yang J.,** *Modified GTAW Welding Joint Process: An Approach to Improve Microstructure and Fracto-Mechanical Behavior by MWCNTs Inducement in Al-Mg-Si Alloy*, Materials, 2019, vol. 12, iss. 9, 1441.
[25] **Wang J., Pan Z., Wang Y., Wang L., Su L., Cuiuri D., Zhao Y., Li H.,** *Evolution of crystallographic orientation, precipitation, phase transformation and mechanical properties realized by enhancing deposition current for dual-wire arc additive manufactured Ni-rich NiTi alloy*, Additive Manufacturing, 2020, vol. 34, 101240.
[26] **Xie J., Zhou Y., Zhou C., Li X., Chen Y.,** *Microstructure and mechanical properties of Mg–Li alloys fabricated by wire arc additive manufacturing*, Journal of Materials Research and Technology, 2024, vol. 29, pp. 3487-3493.
[27] **Chen Y., Sun S., Zhang T., Zhou X., Li S.,** *Effects of post-weld heat treatment on the microstructure and mechanical properties of laser-welded NiTi/304SS joint with Ni filler,* Materials Science and Engineering: A, 2020, vol. 771, 138545.
[28] **Chen Y., Mao Y., Lu W., He P.,** *Investigation of welding crack in micro laser welded NiTiNb shape memory alloy and Ti6Al4V alloy dissimilar metals joints,* Optics & Laser Technology, 2017, vol. 91, pp. 197-202.
[29] **Shao L., Zhang S., Hu L., Wu Y., Huang Y., Le P., Dai S., Li W., Xue N., Xu F., et al.,** *Influence of Heat Treatment Condition on the Microstructure, Microhardness and Corrosion Resistance of Ag-Sn-In-Ni-Te Alloy Wire*, Materials, 2024, vol. 17, 2785.
[30] **Soltani H. M., Tayebi M**., *Comparative study of AISI 304L to AISI 316L stainless steels joints by TIG and Nd:YAG laser welding,* Journal of Alloys and Compounds, 2018, vol. 767, pp. 112-121.
[31] **Rajaravi C., Ganesh B., Lakshmanan S., Gobalakrishnan B.,** *Influence of TIG welding processing parameters on mechanical properties of austenitic stainless steel using Taguchi analysis.* Materials Today: Proceedings, 2022, vol. 72, pp. 2402-2409.
[32] **Ghumman K. Z., Ali S., Khan N. B. et al.,** *Optimization of TIG welding parameters for enhanced mechanical properties in AISI 316L stainless steel welds,* International Journal of Advanced Manufacturing Technology, 2025, vol. 136, pp. 353-365.
[33] **Ahmadi E., Ebrahimi A. R.,** *Welding of 316L Austenitic Stainless Steel with Activated Tungsten Inert Gas Process*, J. of Materi Eng and Perform, 2015, vol. 24, pp. 1065-1071.
[34] **Sharma P., Dwivedi D. K.,** *A-TIG welding of dissimilar P92 steel and 304H austenitic stainless steel: Mechanisms, microstructure and mechanical properties,* Journal of Manufacturing Processes, 2019, vol. 44, pp. 166-178.
[35] **Baghel A., Sharma C, Upadhyay V. et al.,** *Optimization of process parameters for autogenous TIG welding of austenitic stainless-steel SS-304*, International Journal on Interactive Design and Manufacturing, 2024, vol. 18, pp. 6709-6723.
[36] **Tseng K.-H., Hsu C.-Y.,** *Performance of activated TIG process in austenitic stainless-steel welds,* Journal of Materials Processing Technology, 2011, vol. 211, iss. 3, pp. 503-512.
[37] **Kumar H., Singh N.K.,** *Performance of activated TIG welding in 304 austenitic stainless-steel welds,* Materials Today: Proceedings, 2017, vol. 4, iss. 9, pp. 9914-9918.